Macromolecules
ARTICLE

Macromolecules **2010**, *43*, 6075–6084 **6075**
DOI: 10.1021/ma1008786

Free Volume Investigation of Polymers of Intrinsic Microporosity (PIMs): PIM-1 and PIM1 Copolymers Incorporating Ethanoanthracene Units

Thomas Emmler,[†] Kathleen Heinrich,[†] Detlev Fritsch,*[,†] Peter M. Budd,*[,‡] Nhamo Chaukura,[‡] Dennis Ehlers,[§] Klaus Rätzke,*[,§] and Franz Faupel[§]

[†]*GKSS-Forschungszentrum Geesthacht GmbH, Institut für Polymerforschung, Max-Planck-Strasse 1, 21502 Geesthacht, Germany,* [‡]*Organic Materials Innovation Centre, School of Chemistry, University of Manchester, Manchester M13 9PL, U.K., and* [§]*Technische Fakultät der Universität Kiel, Institut für Materialwissenschaft, Materialverbunde, Kaiserstrasse 2, 24143 Kiel, Germany*

Received April 20, 2010; Revised Manuscript Received June 8, 2010

ABSTRACT: High free volume, film-forming copolymers were prepared in which a proportion of the spiro-units of PIM-1 were replaced with units derived from 9,10-dimethyl-9,10-dihydro-9,10-ethanoanthracene-2,3,6,7-tetrol (CO1). A full investigation of free volume, utilizing N_2 sorption, positron annihilation lifetime spectroscopy (PALS), Xe sorption and ^{129}Xe NMR spectroscopy, was undertaken for copolymer PIM1-CO1-40 (spiro-units:CO1 = 60:40) and a comparison is made with PIM-1. All techniques indicate that the copolymer, like PIM-1, possesses free volume holes or pores on the nanometre length scale (i.e., microporosity as defined by IUPAC). For the batch of PIM-1 studied here, the sample as received showed anomalous N_2 sorption, Xe sorption and ^{129}Xe NMR behavior that could be interpreted in terms of reduced porosity in the size range 0.6−0.7 nm, as compared to the copolymer. The anomalous behavior was eliminated on conditioning or relaxation of the polymer, *e.g.*, by Xe sorption at 100 °C and 3 bar. PALS for both PIM1-CO1-40 and PIM-1 indicates a maximum in the average free volume hole size, and in the width of the distribution of hole sizes, on increasing temperature. This maximum appears to be a feature of high free volume polymers and may be related to the onset of localized oscillations of backbone moieties.

Introduction

The advent of soluble polymers of intrinsic microporosity (PIMs) in 2004[1−5] attracted high interest in the polymer community, especially in membrane science, because of their superior transport properties for gases, vapors, and liquids.[3,6−10] PIMs fall into the class of high free volume polymers, with a detectable fractional free volume above 20%. This class of polymers was first detected by Masuda[11] in his pioneering research with polyacetylenes. To date, only a very few membrane polymers or classes of polymers have been found that fall within this category: polyacetylenes such as polytrimethylsilylpropyne (PTMSP)[11] or indane based polyacetylenes,[12] tetrafluoroethylene copolymers with cyclic, perfluorinated 1,3-dioxole units such as Teflon AF and Hyflon AD, some fluorinated polyimides,[8,13−15] and polynorbornenes.[16] Membrane materials are commonly subdivided into porous and nonporous (homogeneous) materials, which have different transport and separation mechanisms. For porous materials, as the pore diameter decreases, there is increasing interaction of the penetrants with the pore walls, rather than each other, giving rise to Knudsen flow. With homogeneous materials, e.g., polymers without interpenetrating pores, the penetrants have to dissolve in the polymer and pass through the chain network by an activated diffusion process. This solution/diffusion mechanism results in much higher selectivity for separation of gases and vapors. High free volume polymers are in between homogeneous and porous materials, as detected some time ago for PTMSP,[17] with a transport mechanism that may be considered to involve both pore diffusion and solution/diffusion.

The aim of this paper is to analyze PIM polymers in respect to their free volume. PIMs are characterized by their ladder structure with sites of contortion, resulting in good solubility on the one hand and hindered packing on the other hand, providing high free volume and permeability. The archetypal PIM is PIM-1, which is prepared from the tetrahydroxy monomer 5,5′,6,6′-tetrahydroxy-3,3,3′,3′-tetramethyl-1,1′-spirobisindane (TTSBI) and the fluoro-monomer 1,4-dicyanotetrafluorobenzene (DTFB) by a step polymerization involving a double aromatic nucleophilic substitution (Scheme 1).

One might expect that the combination of stiff sites of contortion with a ladder structure would result in brittle films, if any films are formed. The remarkable flexibility of PIM films can be understood in the light of a molecular modeling study of PIM-1,[18] as some flexibility of the site of contortion (spiro-center) and some flexing of the dioxane rings out of plane were seen in the packed structure. As already pointed out in the basic patent,[19] other monomers may be used to yield PIMs, instead of the tetrahydroxyspirobisindane used in PIM-1. However, with almost all other tetrahydroxy units, only low molecular weight, brittle polymers could be synthesized. Our approach was to form random copolymers incorporating a relatively rigid tetrahydroxy unit, 9,10-dimethyl-9,10-dihydro-9,10-ethanoanthracene-2,3,6,7-tetrol (CO1, Scheme 1), in increasing amounts.[7]

The monomer CO1 is characterized by a roof-like shape induced by the ethano bridge (see Figure 1) over the middle ring. Thus, CO1 introduces a "bend" into the polymer structure, but we can expect it to be less flexible, at least in some directions, than a spiro-center, which involves a single tetrahedral carbon atom. This should modify the packing of the polymer chains and so affect the free volume.

Motivated by earlier results[20,21] that showed a very unusual behavior of PIM-1 in temperature dependent positron annihilation lifetime spectroscopy (PALS) measurements, we sought to investigate further the behavior of PIM-1 and related polymers

*Corresponding authors. E-mail: (D.F.) fritsch@gkss.de; (P.M.B.) Peter.Budd@manchester.ac.uk; (K.R.) kr@tf.uni-kiel.de.

Published on Web 06/21/2010

Scheme 1. Preparation of PIM-1 from 5,5′,6,6′-Tetrahydroxy-3,3,3′3′-tetramethyl-1,1′-spirobisindane (TTSBI) and 1,4-Dicyanotetrafluorobenzene (DTFB) and of PIM1-CO1-*xx* Copolymers from TTSBI, DTFB, and 9,10-Dimethyl-9,10-ethano-9,10-dihydro-2,3,6,7-tetrahydroxyanthracene (CO1)

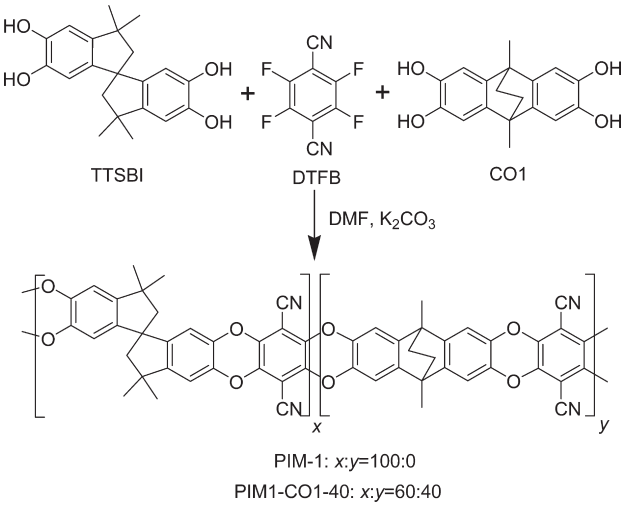

using different analytical methods. Partially replacing the relatively flexible spiro-centers of PIM-1 with a more rigid unit should lead to a material with subtly different properties, reflecting changes in the free volume and so revealing differences in the "creation" and stabilization of the free volume. Evaluation of the effects of introducing the comonomer CO1 into the PIM-1 structure can be done by measuring the pore sizes of the polymer samples with different methods. Here, ^{129}Xe NMR and PALS are sensitive for the local structures and N_2 and Xe sorption will give a more integrated view into the sample.

In the amorphous state, apart from the interstitial free volume, which is also present in the crystalline state, a material contains a hole free volume as well. It typically lowers the density by about 10% in the amorphous state, as compared to the crystalline material. This kind of free volume appears in the form of many irregularly shaped local free volume elements (denoted as holes) of atomic and molecular dimensions, which arise because of disordered, static or dynamic, molecular packing. The dynamics in small molecule glass formers, as observed in mechanical or dielectric relaxation and in viscosity experiments, are related to this type of (excess or hole) free volume.[22−25] Only limited experimental information about the hole free volume and its microstructure is available. Frequently, this free volume (V_f) is calculated as the difference between the total and a zero point volume, which is estimated from the extrapolation of the densities of crystalline or liquid materials at 0 K.[23,26] A value of

$$V_f = V - 1.3V_W \quad (1)$$

where V is the specific volume of the polymer and V_W is the specific van der Waals volume, is commonly accepted. In a high free volume polymer, such as a PIM, there may be sufficient interconnectivity of free volume for it to be regarded as a microporous material according to the IUPAC definition (pore size < 2 nm).[27]

Positron annihilation lifetime spectroscopy (PALS) appears to be one of the most suitable experimental tools to characterize the hole free volume in amorphous dielectrics such as polymers and low molecular weight organic materials. In this technique, positronium in its ortho-state, *o*-Ps, is used as a probe for local free volume holes.[28−37]

^{129}Xe NMR spectroscopy has proven to be a valuable tool for the determination of pore sizes in inorganic materials like, e.g., zeolites[38−41] and polymers, including high free volume polymers such as Teflon AF-types.[42−44]

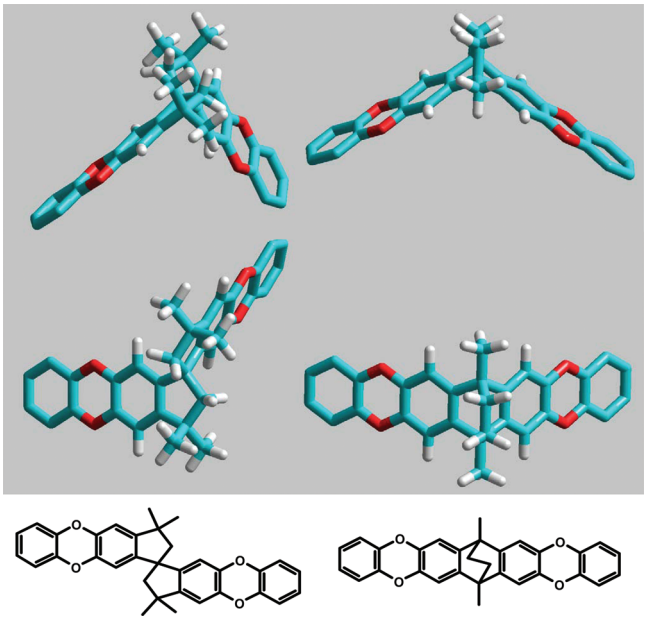

Figure 1. Sterical orientation of chain fragments arising from the two tetrahydroxymonomers used for PIM-1 (left side: from 5,5′,6,6′-tetrahydroxy-3,3,3′3′-tetramethyl-1,1′-spirobisindane) and PIM1-CO1-40 (right side: from 9,10-dimethyl-9,10-dihydro-9,10-ethanoanthracene-2,3,6,7-tetrol). An additional benzene ring is added to the structure to guide the eye.

N_2 sorption and Xe sorption are known to be the method of choice when determining the free volume and pore sizes of porous media. Since a xenon atom is much larger than a nitrogen atom, the surface and hole sizes "seen" by these two different probes are different.

Using all techniques together should result in a deeper understanding of the relationship of structure to properties of high free volume polymers.

Experimental Section

Polymers. PIM-1 (batch CT/02/07) was synthesized by polycondensation of 1,4-dicyanotetrafluorobenzene with 5,5′,6,6′-tetrahydroxy-3,3,3′,3′-tetramethyl-1,1′-spirobisindane in DMF and K_2CO_3 as described previously.[45] PIM-1 random copolymers with various contents of 9,10-dimethyl-9,10-dihydro-9,10-ethanoanthracene-2,3,6,7-tetrol[46] were prepared similarly in nearly quantitative yield[7] and are designated as PIM1-CO1-zz, where zz stands for mol % CO1 of the tetrahydroxy monomers. The copolymers form flexible, free-standing films up to a CO1 content of 50%, very much comparable to PIM-1. The copolymers above 50% of CO1 were characterized only by N_2 sorption. PIM-1 and PIM1-CO1-40 from the same batch were used for all experiments.

N_2 Adsorption/Desorption at 77 K. An accelerated surface area and porosimetry (ASAP) 2020 system from Micromeritics Instrument Corporation (Norcross, GA) was used for N_2 sorption analysis. The sample was first degassed under ultra high vacuum (10^{-9} bar) at a temperature of 120 °C for 16 h, then transferred to the analysis system under nitrogen and again degassed under ultra high vacuum at a temperature of 120 °C overnight. Sorption and desorption analysis was carried out at liquid nitrogen temperature (−196 °C). Free-space determination was carried out after sorption analysis, using He at ambient temperature and −196 °C. Apparent surface areas were calculated from N_2 adsorption data by the multipoint Brunauer−Emmet−Teller (BET) method. The area per N_2 molecule at −196 °C was taken as 0.162 nm^2. Apparent micropore distributions

were calculated from N_2 adsorption data by the Horvath−Kawazoe (HK) method,[47] assuming a slit-pore geometry and the original HK carbon−graphite interaction potential.

Positron Annihilation Lifetime Spectroscopy (PALS). PALS was performed using ^{22}Na as a positron source in the setup described earlier in detail.[37,48] Temperature dependent PALS measurements were carried out with PIM-1 and PIM1-CO1-40 in the form of stacked films of about 1 cm in total height. In particular, we compared as prepared samples with samples stored in methanol for 24 h and dried again to establish a well-defined, relaxed state. As the as-prepared samples showed non-reproducible results during the first heating (probably due to evaporation of species adsorbed from the atmosphere) only the second heating run is shown. These temperature runs were then reproducible within mean error margins.[20]

The data were evaluated using the established program LT (LT for LifeTime, Version 9.0 from J. Kansy). This program allows one to use a dispersion σ_3 in the o-Ps lifetime τ_3, taking into account a distribution of hole sizes, as expected for amorphous polymers. For the detailed overview of the features of the software see reference.[49] With a count rate of typically 200 cts/s, altogether 5×10^6 cts were summed up and evaluation of data was done with two resolution functions and a fixed lifetime $\tau_1 =$ 125 ps.

Xe Adsorption. Xe sorption was measured for the same pressure range as for the ^{129}Xe NMR experiments (see below) using magnetic suspension balances from Rubotherm. The glass version was applied for measurements up to 1.5 bar, the metal version up to 3 bar of Xe pressure. The samples (300 mg PIM-1 and 100 mg PIM1-CO1-40) were sealed into a polyphenylene-sulfide (PPS) fleece and dried at 120 °C in an oil-free high vacuum for at least 12 h to desorb any possible condensable contaminants. No significant sorption for the PPS fleece to Xe was detected. After transfer into the magnetic scale the samples were dried again overnight in an oil-free high vacuum. Typically, 15 min were sufficient to obtain no further mass uptake after setting the Xe pressure, starting from high vacuum.

^{129}Xe NMR. For ^{129}Xe NMR the samples were placed in special pressure-stable NMR tubes (Wilmad). Prior to the NMR experiments, the samples were heated to 120 °C at oil-free high vacuum for at least 12 h to desorb any possible accumulated vapors. For sample preparation, the sample-filled NMR tube was attached to a vacuum/pressure line fitted with a cooling/warming bath for the sample tube that allowed adjustment of the Xe pressure over the sample from 0 to ca. 3 bar at the given temperature. Xenon from Messer, quality 4.0 with water content <5 ppm, was applied. After equilibrium sorption of Xe, obtained by stable Xe gas pressure for more than 15 min, the sample was rapidly transferred into the NMR magnet and there another 15 min were allowed for temperature equilibration. All ^{129}Xe NMR experiments were performed on a Bruker Avance NMR Spectrometer operating at a field of 7 T (83.03 MHz for ^{129}Xe). The spectra were recorded applying 30° pulses (5 μs); the repetition time was chosen in such a way that the sample was fully relaxed. The chemical shifts given are relative to Xe gas at 25 °C and 1 bar as an external standard. For further data treatment, see Results and Discussion.

Results and Discussion

N_2 Adsorption/Desorption. Table 1 gives BET surface areas from N_2 adsorption for copolymers with various proportions of comonomer CO1 and for the PIM-1 (batch CT/02/07) used in subsequent studies. Most of these results fall within the range of values observed for PIM-1 from different batches or with different thermal histories (720−780 $m^2\ g^{-1}$). The polymer without any spiro-units, PIM1-CO1-100, showed a slightly lower surface area of 630 $m^2\ g^{-1}$. This polymer was of low molar mass and did not form films.

The copolymer PIM1-CO1-40 was selected for further study. Figure 2a compares the N_2 adsorption/desorption isotherms at liquid nitrogen temperature (−196 °C) for PIM1-CO1-40 and PIM-1. Both polymers show high uptake at very low relative pressure, characteristic of a microporous material as defined by IUPAC (pore size <2 nm).[27] Both materials also exhibit hysteresis, the desorption curve lying above the adsorption curve down to low relative pressures, which is typical of microporous polymers and may be attributed to swelling effects. Analysis of the very low relative pressure regions of the adsorption isotherms by the Horvath−Kawazoe (HK) method (discussed further in the context of Xe adsorption below) gives the pore size distributions shown in Figure 2b. Both polymers exhibit a broad distribution of effective pore size in the micropore region. The apparent peak at 0.6 nm corresponds to the lowest pressure experimentally achievable with a turbomolecular pump and includes a contribution from smaller pores. The significant difference between the two samples is that the PIM-1 shows lower uptake over a pressure range that, according to the HK model used, represents pores in the size range 0.65−0.7 nm. It is the apparently "missing" porosity in this size range that leads to a lower total uptake of N_2 (Figure 2a) and a lower BET surface area (Table 1). This

Table 1. BET Surface Area, S_{BET}, of PIM-1 and Its Copolymers with Ethanoanthracene Unit CO1

polymer	ratio spiro-unit:CO1	$S_{BET}/(m^2\ g^{-1})$
PIM-1 batch CT/02/07	100:0	720
PIM1-CO1-40	60:40	760
PIM1-CO1-50	50:50	790
PIM1-CO1-61	39:61	720
PIM1-CO1-100	0:100	630

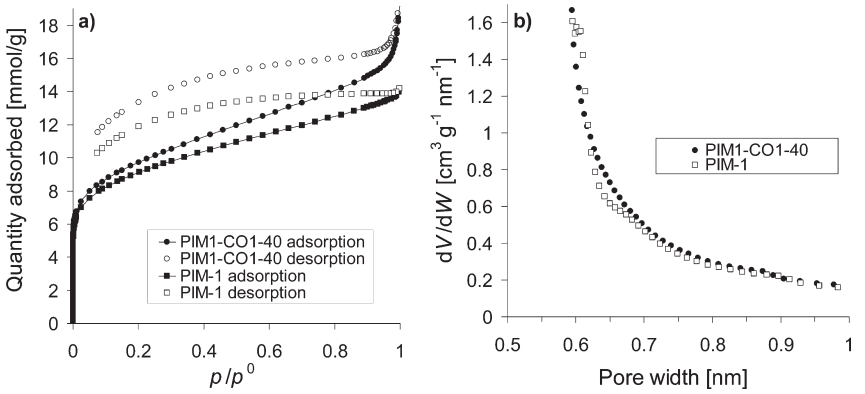

Figure 2. (a) N_2 adsorption (filled symbols) and desorption (open symbols) isotherms at −196 °C for PIM1-CO1-40 (●, ○) and PIM-1 batch CT/02/07 (■, □) and (b) pore width distributions obtained by analysis of N_2 adsorption at −196 °C by the Horvath−Kawazoe method.

point will be discussed further below, in the context of Xe adsorption.

Positron Annihilation Lifetime Spectroscopy. PALS is an extremely useful method for examination of the free volume of polymers. A successful quantum mechanical model for the calculation of free volume hole sizes has been developed by Tao.[50] In this model, the positronium is assumed to be confined in a sphere and a potential well with infinite wall height. For such a problem, the Schrödinger equation can be formulated and solved analytically. Furthermore, the model postulates an electron layer at the pore wall, with which the orthopositronium can interact and decay. Calculation of the overlap integral of the positronium probability density function with this electron layer yields a direct relation between positronium lifetime and the hole radius:

$$\tau_{o-Ps} = \lambda_0^{-1}\left(1 - \frac{R_h}{R_h + \delta R} + \frac{1}{2\pi}\sin\frac{2\pi R_h}{R_h + \delta R}\right) \qquad (2)$$

This formula includes the reciprocal orthopositronium decay rate $\tau_{o\text{-}Ps}$, the spin averaged decay rate in the electron layer λ_0, the hole radius R_h, and the thickness of the electron layer δR. This has been used first by Eldrup[51] and the latest calibration using substances with known pore sizes is by Jean.[28,52]

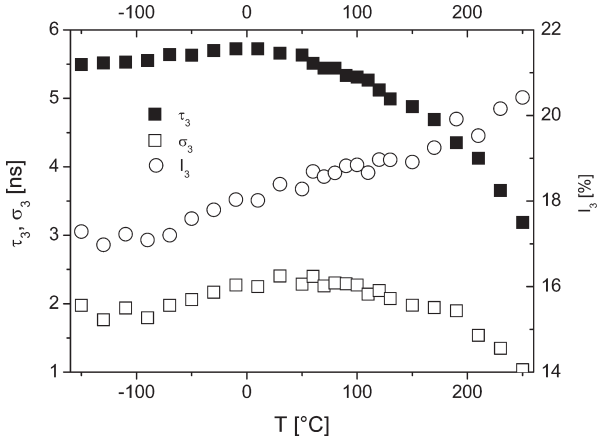

Figure 3. Temperature dependence of o-Ps lifetime τ_3, dispersion σ_3 and intensity I_3 of PIM1-CO1-40. Note the maximum in τ_3 at approximately 0 °C.

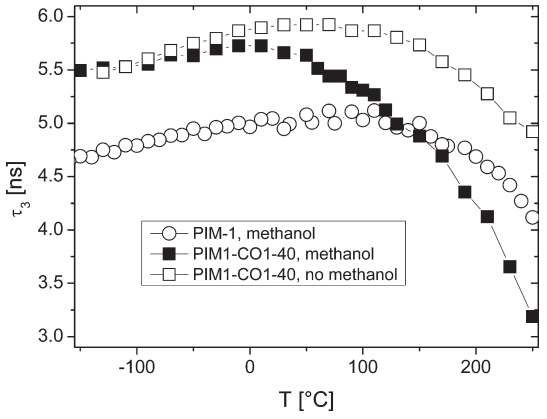

Figure 4. Comparison of o-Ps lifetime τ_3 as a function of temperature for PIM-1 and PIM1-CO1-40 methanol-treated to be in a well-defined, relaxed state, and the PIM1-CO1-40 also without methanol treatment for comparison.

Table 2. Lifetimes, τ_1, τ_2, and τ_3, and Dispersion of Lifetimes, σ_1, σ_2, and σ_3, for PIM1-CO1-40 (Methanol Treated)[a]

PIM1-CO1-40	τ_1 (ns)	τ_2 (ns)	σ_2 (ns)	τ_3 (ns)	σ_3 (ns)
−150 °C (min *T*)	0.125	0.46 ± 0.01	0.08 ± 0.01	5.49 ± 0.04	1.97 ± 0.07
50 °C (≈maximum)	0.125	0.45 ± 0.01	0.12 ± 0.01	5.63 ± 0.04	2.28 ± 0.07
250 °C (max *T*)	0.125	0.44 ± 0.01	0.16 ± 0.01	3.18 ± 0.03	1.03 ± 0.06

[a] Only τ_1 was fixed for fitting.

Figures 3 and 4 show the results for the polymers investigated here. As discussed above, only the second, reversible run for each sample is shown. In Figure 3, the temperature dependence of the o-Ps lifetime τ_3, reflecting the average hole size (see eq 2), and σ_3, reflecting the width of the distribution of hole sizes, is shown for a sample of PIM1-CO1-40 which had been methanol-treated to give a defined, relaxed state. It can be seen that τ_3 and σ_3 go through a smooth maximum in the range between 0 and 50 °C. In Figure 4, the o-Ps lifetime for methanol-treated PIM1-CO1-40 is compared with untreated PIM1-CO1-40 and methanol-treated PIM-1. All three samples show a maximum in τ_3, although the position of the maximum varies. Methanol treatment, i.e., relaxation of the sample, decreases the lifetime τ_3 at higher temperatures, shifting the maximum to a lower temperature.

In the following, we will first give values for the average hole size derived from eq 2, for a comparison with other methods discussed later. Then, we will discuss some possible reasons for the unusual temperature dependence, which seems to be a general feature of polymers with high free volume.

Of the three lifetimes given in Table 2, only τ_3 contains information about the free volume itself (τ_1 stems from the singlet state parapositronium, τ_2 is produced by those positrons which did not find a free electron for positronium formation and decay as "free" positrons). Using the Tao model (eq 2), it is possible to derive pore diameters (for spherical holes) from PALS data. Table 3 contains the comparison of PALS data for spherical holes of PIM-1 and its copolymer.

For a detailed discussion on the unusual temperature behavior, first experimental artifacts will be excluded and then the possibility of local, thermally activated movements reducing the size of the free volume will be discussed.

As the intensity I_3 does not show any extraordinary behavior in this temperature range, we can exclude any artifacts originating from changes in o-Ps formation or quenching, As the dispersion σ_3, reflecting the width of the distribution of holes, shows the same behavior as the average value τ_3, any artifacts from the evaluation or from a change

Table 3. Orthopositronium Lifetime, τ_3, and Diameter of Spherical Holes, D_h, Derived Using eq 2, for PIM-1 and PIM1-CO1-40

T [°C]	τ_3 for PIM-1 (MeOH) [ns]	D_h for PIM-1 (MeOH) [Å]	τ_3 for PIM1-CO1-40 (no MeOH) [ns]	D_h for PIM1-CO1-40 (no MeOH) [Å]	τ_3 for PIM1-CO1-40 (MeOH) [ns]	D_h for PIM1-CO1-40 (MeOH) [Å]
−150	4.69	9.2	5.47 (−130 °C)	9.93	5.49	9.95
−25	4.96	9.5	5.81	10.22	5.71	10.14
+25	4.98	9.46	5.92	10.31	5.69	10.12
+50	5.02	9.48	5.92	10.31	5.63	10.07
+100	5.02	9.52	5.86	10.26	5.30	9.78
+250	4.11	8.61	4.92	9.43	3.18	7.52

in the shape of the hole size distribution can be excluded as well.

The present behavior resembles the curves recently found for PIM-1 and PIM-7[20] in having this unusual maximum. Published data only rarely detected a decrease in lifetime with increasing temperature.[53−55] In these papers the high free volume fluorinated Teflon AF[53−55] and Cytop[55] polymers were analyzed. Out of the two Teflon AF types, only the grade 2400 with the higher comonomer and free volume content showed this lifetime decrease at elevated temperature and the Cytop polymer only after a gas exposure to 2000 bar CO_2. A comparison of lifetime with increasing temperature in Figure 4 illustrates the similar characteristics of PIM-1 and its copolymer PIM1-CO1-40.

Although we have no macroscopic thermal expansion measurements for the PIM1 copolymer, published data for the PIM-1 and for the Teflon AF show normal behavior in the length direction of the film. A possible asymmetric expansion could not be detected by the applied methods. Asymmetric expansion is seen during the methanol treatment: Shrinking in length by about 10−20% and increasing in thickness by 5−10%, thus demonstrating an asymmetry during chain relaxation by methanol.

Concerning the unusual temperature dependence of the o-Ps lifetime, one can only speculate. In a similar investigation on Teflon AF,[53] a comparison of Teflon AF 1600 (regular behavior) and Teflon AF 2400 (unusual behavior as here) allowed us to exclude any artifacts from positronium formation or of the experimental technique. The tentative explanation in that investigation was centered around increasing mobility of the rings of 2,2-bis(trifluoromethyl)-4,5-difluoro-1,3-dioxole that form main chains in Teflon AF 2400. They can exist in two conformations[56] with different distortions of the flat shape and hence increasing temperature can cause local movements reducing the size of the free volume holes of the ring. In an analogous way, one could assume here that the oxygen atoms in the dioxane ring start oscillating out of plane with increasing temperature. This oscillation should set in at the maximum temperature of τ_3 (see Figure 4). If we take this assumption seriously, the different maximum temperatures for the different PIM derivatives (PIM-1, PIM-7, PIM1-CO1-40) can be related to the ratio of spiro-centers to dioxane rings, resulting in more load to the spiro-centers in PIM1-CO1-40 than in PIM-1. Also, methanol-treated samples, where the chain structure is relaxed from film forming stress and residual solvent or adsorbed vapors are removed, show higher free volume, which affects the mobility of dioxane moieties.

Xe Adsorption. Xenon adsorption was measured in the range of the ^{129}Xe NMR experiments (0−3 bar), to verify a steady, "normal" increase as expected for an easily condensable gas following a dual mode sorption curve.[57] Table 4 gives the order of the measurements to document the sample history, as an irreversible aging of the PIM-1 sample by Xe at 100 °C was detected.

Before measurement, all samples were carefully desorbed of any moisture adsorbed from the atmosphere by heating overnight in an oil-free high vacuum at 120 °C. After mounting in the sorption balance, the sample was again desorbed overnight in high vacuum. For PIM-1, the sorption curves at 85 °C, and especially at 25 °C (Figure 5), showed an unexpected inflection in the range 10 to about 1500 mbar. PIM1-CO1-40 displayed nonideal Xe uptake only to some extent in the region below 100 mbar at 85 °C. The adsorption at 100 °C (merely 15 °C higher than the first measurement) followed the expected behavior up to 3 bar. Going back to 25 °C, after careful evacuation, both polymers followed the expected adsorption behavior.

Table 4. Order of Xe Sorption Measurements

no.	PIM-1 (°C)	PIM1-CO1-40 (°C)
1	85	85
2	25	25
3	100	100
4	25	25
5	25	-

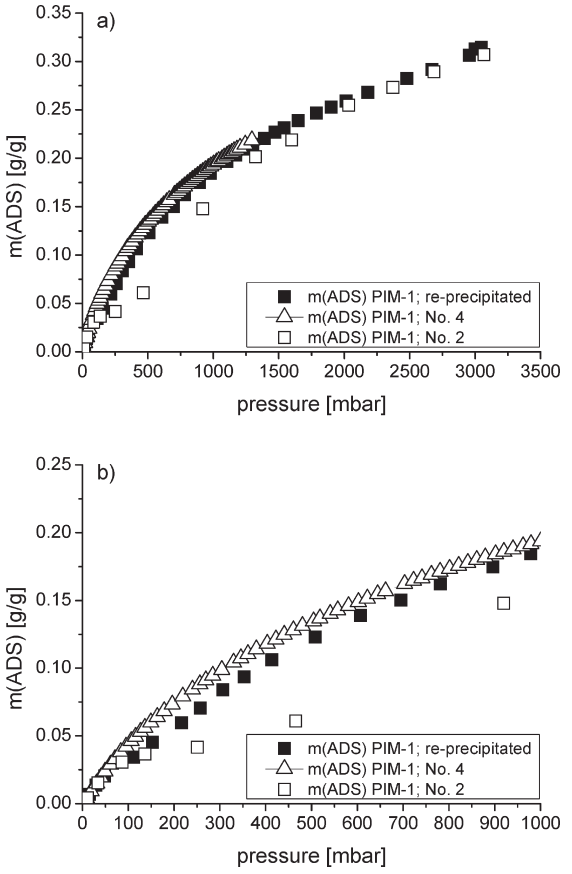

Figure 5. Sorption of Xe on PIM-1 at the second (□) and forth (△) sorption cycle and after redissolving in $CHCl_3$ and reprecipition in MeOH (■) at 25 °C: (a) complete curve; (b) detail to 1000 mbar. The numbers given for the specific measurements reflect the sample's thermal history (see Table 4).

To validate the aging behavior by Xe adsorption at 100 °C, the PIM-1 sample was redissolved in $CHCl_3$, precipitated into methanol, then dried at 80 °C overnight and at 120 °C in a high vacuum for 12 more hours. The inflection in Xe uptake was recovered, although to a lesser extent, as seen in Figure 5. It thus appears that for this PIM-1 sample an "unrelaxed" structure may be kinetically trapped on precipitation. Differences in the extent of the deviation from expected adsorption behavior may be attributed to minor variations in precipitation conditions and to different aging times after reprecipitation. Xe adsorption at 100 °C presumably plasticizes the sample sufficiently for relaxation to occur.

Xe adsorption isotherms at 25 °C for "relaxed" samples of PIM-1 and PIM1-CO1-40 (i.e., after Xe adsorption at 100 °C) are shown in Figure 6, together with adsorption data from the literature for PPO and PTMSP.[58,59] The previously found higher sorption characteristic of PIM polymers for light gases is also detected for Xe and reported in comparison to other highly permeable polymers in Table 5. PIM polymers adsorb about two times more Xe than PTMSP and roughly three times more than PPO.

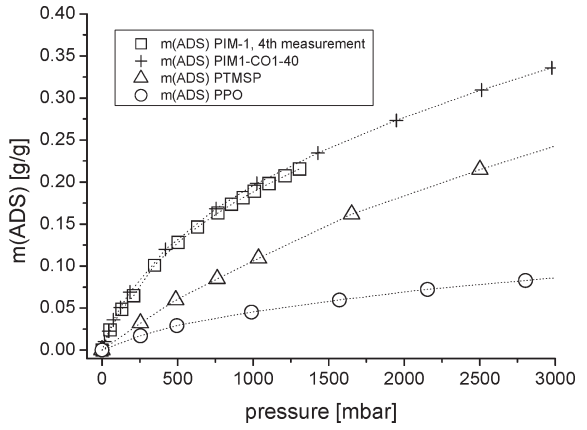

Figure 6. Comparison of Xenon sorption curves of PIM-1, PIM1-CO1-40 (both after 100 °C Xe-sorption), PTMSP,[60] and PPO at 25 °C.[58].

Table 5. Amount of Adsorbed Xe at 1000 and 2000 mbar and 25 °C by PIM Polymers in Comparison to PTMSP and PPO (PTMSP and PPO Calculated from Refs 58 and 59)

	Xe (ADS) [g/g] (% of PIM-1)			
pressure [mbar]	PIM-1	PIM1-CO1-40	PTMSP	PPO
1000	0.194 (100)	0.196 (100)	0.106 (54)	0.060 (30)
2000	0.279 (100)	0.277 (100)	0.185 (66)	0.097 (35)

Adsorption data may be analyzed in various ways. First, as with the low pressure N_2 adsorption data discussed above, the Horvath−Kawazoe (HK) method may be applied; this treats the polymer as a rigid, microporous material with a distribution of pore sizes. Second, the dual-mode sorption model may be applied; this is based on the concept that a glassy polymer has both dense regions, in which a penetrant exhibits Henry law behavior, and microvoids, which are associated with a single Langmuir affinity constant. Both these approaches are applied and discussed here.

Horvath−Kawazoe Analysis of Xe Sorption. The Horvath−Kawazoe method[47] assumes that all pores of a particular size will fill at a certain relative pressure. It is applicable to the micropore region (< 2 nm). It was originally derived for slit-shaped pores in a carbonaceous material, but has subsequently been adapted to other pore geometries and types of material.

For slit pores, relative pressure, p/p^o, is related to the distance between the nuclei of two surface layers, l, by

$$RT\ln\left(\frac{p}{p^o}\right) = K\frac{N_a A_a + N_A A_A}{\sigma^4(l-d)} \times\left[\frac{\sigma^4}{3(l-d/2)^3}-\frac{\sigma^{10}}{9(l-d/2)^9}-\frac{\sigma^4}{3(d/2)^3}+\frac{\sigma^{10}}{9(d/2)^9}\right] \quad (3)$$

where R is the gas constant, T is the absolute temperature, K is the Avogadro number, σ is the distance between a gas atom and the nuclei of the surface at zero interaction energy, N_a is the number of atoms per unit area of adsorbent, N_A is the number of atoms per unit area of adsorbate and $d = d_a + d_A$, where d_a is the diameter of an adsorbent atom and d_A is the diameter of an adsorbate molecule. A_a and A_A are given by

$$A_a = \frac{6mc^2\alpha_a\alpha_A}{\frac{\alpha_a}{\chi_a}+\frac{\alpha_A}{\chi_A}} \quad \text{and} \quad A_A = \frac{3mc^2\alpha_A\chi_A}{2} \quad (3a)$$

where m is the mass of an electron, c is the velocity of light, α_a is the polarizability of an adsorbent atom, α_A is the polarizability of an adsorbate molecule, χ_a is the magnetic susceptibility of an adsorbent atom and χ_A is the magnetic susceptibility of an adsorbate molecule. Pore width, w is calculated from l using $w = l - d_a$.

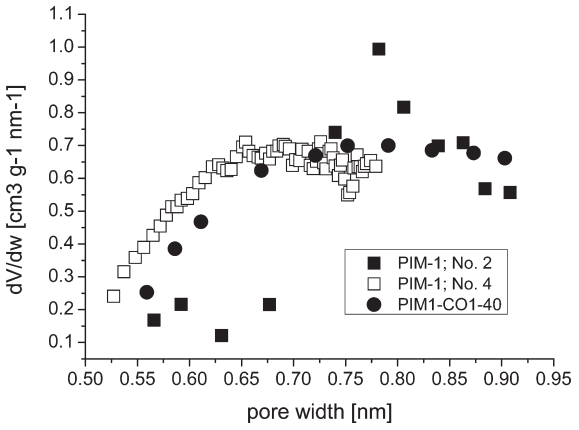

Figure 7. Pore width distributions determined by the Horvath−Kawazoe method from Xe adsorption at 25 °C for PIM1-CO1-40 (●) and for PIM-1 batch CT/02/07 before (■) and after (□) Xe adsorption at 100 °C.

Table 6. Parameters Used in Horvath−Kawazoe Analysis of Xe Adsorption Data at 25 °C

parameter	value	reference
diameter (nm)	0.437	61
polarizability (cm^3)	4.00×10^{-24}	62
magnetic susceptibilty (cm^3)	7.04×10^{-29}	62
no. of atoms per unit area of surface (molecule cm^{-2})	5.30×10^{14}	63
density conversion factor	0.0043	64

Figure 7 shows pore width distributions calculated by the HK method from Xe adsorption data at 25 °C for copolymer PIM1-CO1-40 and for both "unrelaxed" and "relaxed" samples of PIM-1. The parameters used in the calculations are listed in Table 6. For the copolymer, the data suggest a broad distribution of apparent pore size over the range 0.6−1 nm, which is consistent with the results from N_2 adsorption discussed above. "Unrelaxed" PIM-1 is apparently "missing" porosity in the size range 0.55−0.7 nm, as compared to the copolymer or to "relaxed" PIM-1. This is consistent with the conclusions from N_2 adsorption and, as will be seen below, is significant for the interpretation of ^{129}Xe NMR results. The "missing" porosity in an unrelaxed sample could conceivably arise either because larger voids are kinetically trapped on precipitation but subdivide as the polymer relaxes, or because there are densified regions that open up as the polymer relaxes.

Arguably, Figure 7 indicates a distribution of hole size for PIM-1-CO1-40 that is shifted to slightly larger hole sizes than for "relaxed" PIM-1. This may be attributed to the reduced torsional flexibility of the ethanoanthracene unit as compared to the spiro-unit.

Dual Mode Analysis of Xe Sorption. From the Xe sorption data, the dual mode sorption parameters were calculated according to eq 4 by curve fitting and are summarized in Table 7.

$$C = C_D + C_H = k_D p + C_{H'} bp/(1+bp) \quad (4)$$

where C is the equilibrium sorption amount at pressure p, C_D is the concentration of Henry's law contribution, C_H is the concentration of Langmuir mode contribution, k_D is Henry's law constant, b is the affinity constant of Langmuir

Table 7. Dual Mode Sorption Parameters for PIM-1 and PIM1-CO1-40, together with Various Other Polymers for Comparison[a]

polymer	temperature [°C]	$C_{H'}$	$k_D \times 10^2$	$b \times 10^3$	reference
PPO	25	20.6	1.7	7.8	65
TMPC	25	17.4	1.5	6.0	65
PS	25	4.8	1.1	8.8	65
PVTMS	25	18.5	1.2	4.1	66
PTMSP	25	61.7	4.8	4.0	66
PIM-1	25	37.9	13.1	30.8	this paper
PIM1-CO1-40	25	40.2	12.9	27.7	this paper
PIM-1	100	24.6	3.7	3.8	this paper
PIM1-CO1-40	100	76.4	1×10^{-7} [b]	1.9	this paper

[a] Key: $C_{H'}$, [cm^3(STP)/cm^3(polym.)]; k_D, [cm^3(STP)/cm^3(polym.) cmHg]; b, [cmHg^{-1}]; PPO = poly(2,6-dimethyl-1,4-phenylene oxide), TMPC = tetramethyl−bisphenol A polycarbonate; PS = polystyrene; PVTMS = poly(vinyl trimethylsilane); PTMSP = poly(trimethylsilyl-propyne). [b] In the curve fit k_D was set to minimum 1×10^{-9} to prevent running into negative values.

sites, and $C_{H'}$ is the Langmuir capacity constant (total sorption capacity in unrelaxed voids).

It can be seen in Table 7 that the data for k_D and b of PIM-1 and PIM1-CO1-40 are much higher compared to normal polymers such as PS, to polymers with higher free volume such as PPO, TMPC or PVTMS, and even to PTMSP, a polymer with one of the highest free volumes reported. This means, both the tendency of Xe to adsorb in Langmuir mode (constant b in eq 4) and to dissolve in the "normal" Henry mode (k_D) is higher for the PIM polymers. However, the total Langmuir capacity represented by $C_{H'}$ is lower than for PTMSP, in accordance to its lower free volume. At 100 °C the Henry contribution to the adsorption shifted to lower values, as did the Langmuir affinity constant. Remarkable is the very high Langmuir capacity constant for PIM1-CO1-40 at 100 °C, even exceeding the value for PTMSP at 25 °C. This points to a change in hole sizes or hole size distribution upon heating.

^{129}Xe NMR. To provide a deeper insight into the behavior of the high free volume PIM polymers, we investigated PIM-1 and the copolymer PIM1-CO1-40 by ^{129}Xe NMR spectroscopy at various pressures and temperatures.

Table 8 provides an overview of reported chemical shifts relative to free Xe in various polymers. In general, the larger the chemical shift, the smaller are the free volume elements, due to the Xe−Xe and Xe-wall collision rates.[67] As the free volume changes considerably at the glass transition temperature, the known high free volume polymers, all in the glassy state at around room temperature, display lower chemical shifts for ^{129}Xe.[42,60,68,69]

Table 9 gives the order of the measurements to document the sample history.

No analyzable signal of free xenon was seen in any of the NMR spectra. As pointed out by Merkel et al.,[60] the NMR signal of free ^{129}Xe decreases with increasing solubility of Xe in the respective polymer. The high solubility of Xe in the present polymers corroborates the observation of a vanishing free ^{129}Xe here.

PIM polymers, which have no detectable glass transition temperature up to 350 °C, exhibit a ^{129}Xe shift of about 160 ppm at 25 °C and 2 bar (Figure 8). For measurements made at 25 °C before carrying out measurements at 100 °C, the PIM-1 sample clearly shows two linear regions in the plot of ^{129}Xe chemical shift against Xe pressure; one from 0.2 to 1.0 bar and another from 2.0 to 2.9 bar, with an unexpected plateau in the pressure range 1 to 2 bar. In contrast, the PIM1-CO1-40 copolymer shows a gradual increase in chemical shift with pressure, without any plateau, comparable to polymers with dual mode sorption behavior.

Table 8. ^{129}Xe NMR Chemical Shift Values of Various Polymers at +25 °C

polymer	shift [ppm]	pressure [bar]	reference
PS	218	10−15	70
LDPE	203	5	71
PPO	180	5	71
PTMSP	178	8	60
PTMSP	147	2	69
AF 2400	69.5	1.5	42

Table 9. Order of NMR Measurements

no.	PIM-1 (°C)	PIM1-CO1-40 (°C)
1	+25	+25
2	+100	+100
3	−25	−25
4	+25	+25

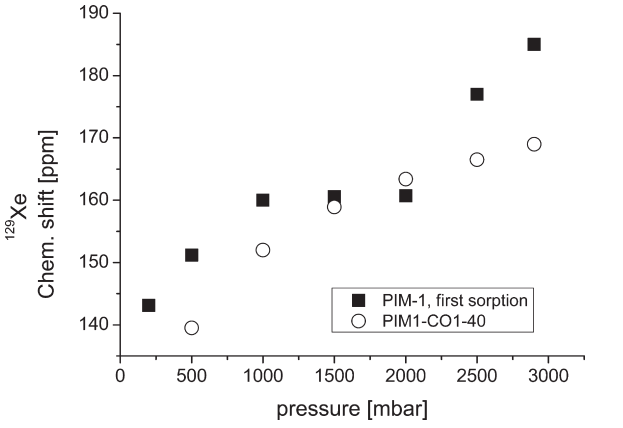

Figure 8. Comparison of the pressure dependent ^{129}Xe chem. Shift at +25 °C for PIM-1 (■) and PIM1-CO1-40 (○), prior to measurements at 100 °C.

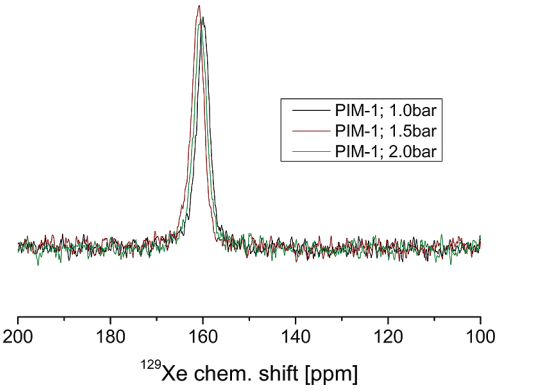

Figure 9. ^{129}Xe NMR spectra of Xe adsorbed on unrelaxed PIM-1 at Xe pressures between 1 and 2 bar over the sample at +25 °C.

For PIM-1, individual ^{129}Xe NMR spectra from the plateau region are superimposed in Figure 9. It is evident that in this region there is little change in the shift, the intensity or the width of the signals. All measurements were performed within 1 day and the Xe pressure on the NMR tube was controlled after each gauging.

In Xe adsorption measurements, as discussed above, it was found that treating the PIM-1 sample under pressure at 100 °C resulted in a "normal" adsorption curve. The effect on the ^{129}Xe NMR spectra is similar (see Figure 10). After measuring the sample at +100 °C with 3 bar Xe pressure, subsequent spectra taken at −25 and +25 °C showed no unexpected features (spectra not shown here).

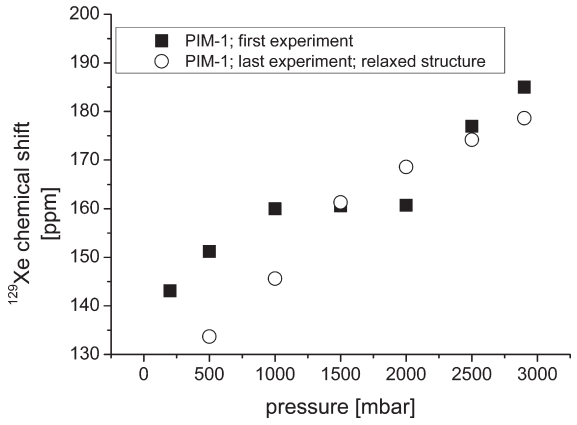

Figure 10. Comparison between the first ^{129}Xe NMR measurement at +25 °C (■) and the measurement at +25 °C after thermal/pressure treatment (○). Please note that the pressure before and after the measurement was checked carefully. A difference in the pressure before and after the measurements of the plateau region in the first measurement was not found. The ^{129}Xe chemical shift for Teflon AF2400 at 2 bar is around 70 ppm,[42] of PTMSP at 147 ppm,[60] and for polystyrene 217 ppm.[72]

We understand that Xe treatment at 100 °C and 3 bar leads to relaxation or conditioning of the polymer and its free volume system, as is well-known, e.g., for conditioning of polymers with CO_2 at high pressures.[65] As discussed above, both N_2 and Xe adsorption data suggest that there is less accessible porosity in the size range 0.6−0.7 nm for unrelaxed PIM-1 than for a relaxed sample. On the basis of the Horvath−Kawazoe parameters in Table 6, for Xe at 25 °C at pressures up to 1 bar pores of width ≤0.75 nm are filled. In this region, the NMR data for unrelaxed PIM-1 extrapolate to a higher chemical shift, corresponding to a smaller pore size, when compared to relaxed PIM-1 (Figure 10) or copolymer PIM1-CO1-40 (Figure 8). At pressures above 2 bar, pores of effective width ≥0.84 nm are filled and the NMR data are consistent with a larger effective pore size.

For the following analysis of the ^{129}Xe NMR spectra at +25 °C only the "relaxed" spectra of the fourth measurement cycle were used.

As shown above from the Xenon sorption experiments, the sorption behavior of Xenon in relaxed PIM-1 and PIM1-CO1-40 may be treated satisfactorily by the dual mode sorption model. The chemical shift of the ^{129}Xe atoms adsorbed in zeolites can be described according to Fraissard and Ito.[40,67] Golemme et al.[42,69] analyzed fluorinated polymers following only Henry sorption and could take over their method of hole size calculation. Suzuki[65,72,73] investigated polymers following dual mode sorption for Xe and developed a method to calculate the hole sizes in glassy polymers and polymer blends by use of the measured ^{129}Xe chemical shift, considering the dual mode sorption. We used the approach of Suzuki et al. The ^{129}Xe chemical shift on polymers is determined by the sum of the possible interactions:[40,67,74−76]

$$\delta_{obs} = \delta(S) + \delta(Xe) + \delta(E) + \delta(SAS) + \delta(M) \qquad (5)$$

The observed chemical shift (see eq 5) is determined by the xenon wall interactions (δ(S)) and the xenon−xenon interactions (δ(Xe)). The residual interactions, δ(E) for the electric field created by cations, δ(SAS) for the shift in strong absorption places and δ(M) for the contribution of the paramagnetic compensation cations, do not play a role for organic polymers like PIM-1 and PIM1-CO1-40.

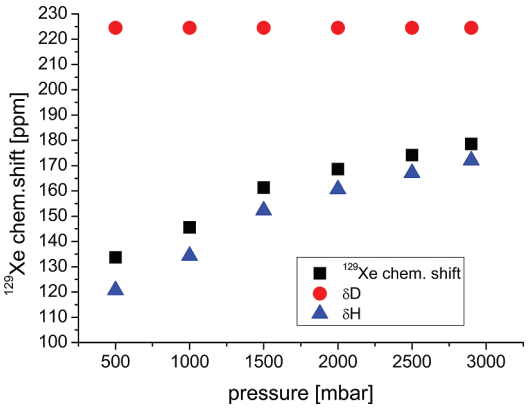

Figure 11. Behavior of the ^{129}Xe chemical shift of the Henry and the Langumir sites in PIM-1 using measurement 4 at +25 °C.

In Suzuki's approach,[65,72,73] the sorption sites are separated into Langmuir and Henry adsorption. The relative concentration of xenon in the sorption sites (C_D and C_H for the Henry and Langmuir sites) is known from the analysis of the xenon sorption curves (see above). The observed chemical shift is interpreted assuming that the chemical shift results from a fast exchange between the Langmuir and Henry sites. Knowing the relative amounts of these sites (ϕ_D and ϕ_H) one can recalculate the chemical shifts (δ_D and δ_H) that characterize them (eq 6).

That means for the observed chemical shift:

$$\delta_{obs} = \phi_D\delta_D + \phi_H\delta_H, \quad \text{when } \phi_D + \phi_H = 1 \qquad (6)$$

The concentration correction due to the shift of free ^{129}Xe with increasing Xe pressure as applied in the Suzuki papers were not implemented, since we work at relatively small pressures (up to 3 bar) and the results with the applied correction at these small Xenon concentrations were within the margin of error. The resulting ^{129}Xe chemical shift vs pressure curves (Figure 11) were fitted using the program "Curve Finder 1.4" with suitable models (e.g., Richardson) to the maximum chemical shift (δ_D) and the δ_H values were calculated using the fit value for δ_D. Using this raw procedure our estimated chemical shifts are off by maybe 5 ppm. Fitting the δ_H vs pressure curve to zero pressure gives the "pure" chemical shift of the Xenon wall interaction ($\delta(S)_H$) and allows calculation of the mean hole size of the polymer that is seen by a Xenon atom by eq 7:[65]

$$\lambda = \frac{243 \times 2.054}{\delta(S)_H} - 2.054 = \frac{D_S - D_{Xe}}{2} \qquad (7)$$

Assuming a most likely error of 5 ppm, we can calculate and give a range for mean free path of a Xenon atom and the diameter for a spherical hole by using a Xe atom diameter (D_{Xe}) of 4.4 Å.[77] Table 10 summarizes the results

For PIM1-CO1-40 at +100 °C, only after an extremely high number of scans was a very broad signal at 125 ppm (2.5 bar) detected. This correlates with the high Langmuir constant and means an interconnected pore system with varying hole sizes is most likely. This value roughly correlates to a value of 8.2 Å, leaving out all corrections, and is in agreement with the data found for PIM-1 treated the same way.

Tables 11 and 12 sum up the hole sizes of PIM-1 and PIM1-CO1-40 found in this work using ^{129}Xe NMR and PALS. PALS measurements of methanol-treated and as-received PIM1-CO1-40 show a slight increase in hole size on

Table 10. Summary of the Hole Diameters Obtained by ^{129}Xe NMR[a]

polymer	temperature [°C]	mean free path of Xe atom [Å]	diameter of spherical hole [Å]
PIM-1	+25	2.8−3.1	10.0−10.7
PIM-1	+100	1.9−2.3	8.2−9.0
PIM1-CO1-40	+25	2.2−2.6	8.8−9.6
PIM1-CO1-40	+100	n.d.	n.d.

[a] Due to the lack of sorption data for −25 °C, the hole sizes for this temperature were not evaluated.

Table 11. Summary of the Structural Data of PIM-1 Obtained by Different Methods (for the Results of N_2 Adsorption/Desorption and Xenon Adsorption, See Text)

temperature [°C]	diameter of spherical hole obtained by NMR [Å]	o-PS lifetime and diameter of spherical hole obtained by PALS (MeOH treated) [Å]	range of pore widths obtained by Xenon adsorption (HK method) [Å]
−150		(4.69 ns) 9.2	
−25	see text	(4.69 ns) 9.5	
+25	10.0−10.7	(4.96 ns) 9.48	6−10
+50		(5.02 ns) 9.48	
+100	8.2 - 9.0	(5.02 ns) 9.52	
+250		(4.11 ns) 8.61	
−150			

Table 12. Summary of the Structural Data of PIM1-CO1-40 Obtained by Different Methods[a]

temperature [°C]	diameter of spherical hole obtained by NMR [Å]	o-PS lifetime and diameter of spherical hole obtained by PALS (MeOH treated) [Å]	range of pore widths obtained by Xenon adsorption (HK method) [Å]
−150		(5.49 ns) 9.95	
−25	see text	(5.71 ns) 10.14	
+25	8.8−9.6	(5.69 ns) 10.12	∼6−10
+50		(5.63 ns) 10.07	
+100	(8.2)	(5.30 ns) 9.78	
+250		(3.18 ns) 7.52	

[a] The value in brackets is only a rough estimation (see text). For the results of N_2 adsorption/desorption and xenon adsorption, see text.

methanol treatment, as has also been reported for PIM-1.[45] All the techniques used in this work support the idea that PIMs contain holes or pores with a size in the region of 10 Å (1 nm).

The PIM1 copolymer, with its torsion-resistant ethanoanthracene unit, displays by PALS nearly 10% increase in hole size compared to PIM-1, consistent with the tentative conclusion from Xe sorption (see above). The ^{129}Xe NMR, however, indicates slightly smaller holes for the copolymer than for PIM-1. The positrons (PALS) and the Xe atoms (^{129}Xe NMR) explore different hole sizes by these methods, thus displaying different packing of PIM-1 and PIM1-CO1-40.

Conclusions

High free volume, film-forming copolymers were prepared in which a proportion of the spiro-units of PIM-1 were replaced by ethanoanthracene (CO1) units. An extensive investigation was carried out of PIM1-CO1-40, which has a 60:40 ratio of spiro-units to CO1 units, and a comparison made with PIM-1. Results from N_2 sorption, PALS, Xe sorption, and ^{129}Xe NMR all indicate that these polymers possess free volume holes or pores on the nanometre length scale (i.e., microporosity as defined by IUPAC). For the batch of PIM-1 studied here, the sample as received showed anomalous N_2 sorption, Xe sorption, and ^{129}Xe NMR behavior that could be interpreted in terms of reduced porosity in the size range 0.6−0.7 nm, as compared to the copolymer. The anomalous behavior was eliminated on conditioning or relaxation of the polymer, *e.g.*, by Xe sorption at 100 °C and 3 bar. In contrast to PIM-1, the copolymer did not exhibit any effects of conditioning by Xe under these conditions. Both PIM1-CO1-40 and PIM-1 show exceptionally high sorption capacities for Xe, greater even than for the highly permeable polymer polytrimethylsilylpropyne (PTMSP).

PALS for both PIM1-CO1-40 and PIM-1 indicates a maximum in the o-Ps lifetime τ_3 (related to average free volume hole size), and in the dispersion σ_3 (related to the width of the distribution of hole sizes), on increasing temperature. The position of the maximum in τ_3 depends on the polymer and on the history of the sample, occurring at ca. 0 °C for methanol-treated PIM1-CO1-40, at ca. 50 °C for PIM1-CO1-40 as received, and at ca. 100 °C for methanol-treated PIM-1. This maximum appears to be a feature of high free volume polymers and may be related to the onset of localized oscillations of backbone moieties.

The introduction of 40 mol % of the torsion-resistant ethanoanthracene unit into PIM-1 resulted in slightly larger hole sizes as explored by PALS.

This work confirms that high free volume polymers exhibit aspects of the behavior both of polymers and of microporous materials. Being glassy polymers, and therefore nonequilibrium, the distribution of free volume, and consequently the sorption and transport properties, can depend markedly on the history of the sample. Suitable treatments with gases (e.g., Xe at 100 °C and 3 bar) or liquids (e.g., immersion in methanol for 24 h) leads to relaxation of the polymer and its free volume system.

Acknowledgment. The authors thank I. Jonas for help in preparing the manuscript. Nhamo Chaukura thanks EPSRC for funding. Dr. Torsten Brinkmann (GKSS) is thanked for discussion and help with calculation of dual mode sorption parameters.

References and Notes

(1) McKeown, N. B.; Budd, P. M. *Chem. Soc. Rev.* **2006**, *35*, 675–83.
(2) Budd, P. M.; McKeown, N. B.; Fritsch, D. *J. Mater. Chem.* **2005**, *15*, 1977–1986.
(3) Budd, P. M.; Elabas, E. S.; Ghanem, B. S.; Makhseed, S.; McKeown, N. B.; Msayib, K. J.; Tattershall, C. E.; Wang, D. *Adv. Mater.* **2004**, *16*, 456–459.
(4) McKeown, N. B.; Budd, P. M.; Msayib, K. J.; Ghanem, B. S.; Kingston, H. J.; Tattershall, C. E.; Makhseed, S.; Reynolds, K. J.; Fritsch, D. *Chem.—Eur. J.* **2005**, *11*, 2610–2620.
(5) Budd, P. M.; Ghanem, B. S.; Makhseed, S.; McKeown, N. B.; Msayib, K. J.; Tattershall, C. E. *Chem. Commun.* **2004**, *2*, 230–231.
(6) Du, N. Y.; Robertson, G. P.; Pinnau, I.; Guiver, M. D. *Macromolecules* **2009**, *42* (16), 6023–6030.
(7) Heinrich, K. *Polymere mit intrinsischer Mikroporosität - Membranmaterialien mit Zukunft?* (*Thesis*). Christian-Albrecht-Universität zu Kiel: Kiel, Germany, 2009.
(8) Robeson, L. M. *J. Membr. Sci.* **2008**, *320* (1−2), 390–400.
(9) Budd, P. M.; Msayib, K. J.; Tattershall, C. E.; Ghanem, B. S.; Reynolds, K. J.; McKeown, N. B.; Fritsch, D. *J. Membr. Sci.* **2005**, *251* (1−2), 263–269.
(10) Fritsch, D.; Heinrich, K.; Bengtson, G.; Pohlmann, J. In *Polymers of intrinsic microporosity: New copolymers, syntheses, properties and applications*; International Congress on Membranes and Membrane Processes, ICOM 2008, Honolulu, HI, **2008**.
(11) Masuda, T.; Isobe, E.; Higashimura, T.; Takada, K. *J. Am. Chem. Soc.* **1983**, *105* (25), 7473–7474.
(12) Hu, Y.; Shiotsuki, M.; Sanda, F.; Freeman, B. D.; Masuda, T. *Macromolecules* **2008**, *41* (22), 8525–8532.
(13) Al-Masri, M.; Kricheldorf, H. R.; Fritsch, D. *Macromolecules* **1999**, *32*, 7853–7858.

(14) Ghanem, B. S.; McKeown, N. B.; Budd, P. M.; Selbie, J. D.; Fritsch, D. *Adv. Mater.* **2008**, *20*, 2766–2771.
(15) Liu, S. L.; Chng, M. L.; Chung, T. S.; Goto, K.; Tamai, S.; Pramoda, K. P.; Tong, Y. J. *J. Polym. Sci., Part B: Polym. Phys.* **2004**, *42*, 2769–2779.
(16) Finkelshtein, E. S.; Makovetskii, K. L.; Gringolts, M. L.; Rogan, Y. V.; Golenko, T. G.; Starannikova, L. E.; Yampolskii, Y. P.; Shantarovich, V. P.; Suzuki, T. *Macromolecules* **2006**, *39*, 7022–7029.
(17) Srinivasan, R.; Auvil, S. R.; Burban, P. M. *J. Membr. Sci.* **1994**, *86* (1−2), 67–86.
(18) Heuchel, M.; Fritsch, D.; Budd, P. M.; McKeown, N. B.; Hofmann, D. *J. Membr. Sci.* **2008**, *318* (1−2), 84–99.
(19) McKeown, N. B.; Budd, P. M.; Msayib, K.; Ghanem, B. *Microporous polymer material and its manufacture*. US 2006 0246273, 2006.
(20) Miranda, R. L. d.; Kruse, J.; Rätzke, K.; Faupel, F.; Fritsch, D.; Abetz, V.; Budd, P. M.; Selbie, J. D.; McKeown, N. B.; Ghanem, B. S. *Phys. Status Solidi RRL* **2007**, *1* (5), 190–192.
(21) Lima de Miranda, R. *Temperature Dependence of the Free Vol. in Polymer of Intrinsic Microporosity* (*PIM*) (*Diplomarbeit*). Christian-Albrechts-Universität zu Kiel: Kiel, Germany, 2006.
(22) Cohen, M. H.; Turnbull, D. *J. Chem. Phys.* **1959**, *31*, 1164–1169.
(23) Doolittle, A. K. *J. Appl. Phys.* **1951**, *22*, 1471–1475.
(24) Turnbull, D.; Cohen, M. H. *J. Chem. Phys.* **1970**, *52*, 3038–&.
(25) Grest, G. S.; Cohen, M. H. *Adv. Chem. Phys.* **1981**, 455−525.
(26) Doolittle, A. K. *J. Appl. Phys.* **1951**, *22*, 1031–1035.
(27) Everett, D. H. *Pure Appl. Chem.* **1972**, *31*, 577–638.
(28) Nakanishi, H.; Wang, S. J.; Jean, Y. C. In *Positron Annihilation Studies of Fluids*; Sharma, S. C., Ed.; World Scientific: Singapore, 1988; p 292.
(29) Mogensen, O. E. *Positron Annihilation in Chemistry*; Springer-Verlag: Berlin, 1995.
(30) Pethrick, R. A. *Prog. Polym. Sci.* **1997**, *22* (1), 1–47.
(31) Bartoš, J. In *Encyclopedia of Analytical Chemistry*; Meyers, R. A., Ed. Wiley: Chichester, U.K., 2000; p 7968.
(32) Dlubek, G. Positron Annihilation Spectroscopy. In *Encyclopedia of Polymer Science and Technology*; Seidel, A., Ed.; John Wiley & Sons: Hoboken, NJ, 2008.
(33) Jean, Y. C.; Mallon, P. E.; Schrader, D. M. Introduction to Positron and Positron Chemistry. In *Principles and Applications of Positron and Positronium Chemistry*; Jean, Y. C., Mallon, P. E., Schrader, D. M., Eds.; World Scientific Press: Singapore, 2003.
(34) Faupel, F.; Kanzow, J.; Günther-Schade, K.; Nagel, C.; Sperr, P.; Kögel, G. In *Positron annihilation spectroscopy*; Materials Science Forum; Hoyodo, T.; Kobayashi, Y.; Nagashima, Y.; Saito, H., Eds.; 2004; pp 445−446.
(35) Dlubek, G.; Shaikh, M. Q.; Krause-Rehberg, R.; Paluch, M. *J. Chem. Phys.* **2007**, *126*, 024906.
(36) Dlubek, G.; Pionteck, J.; Shaikh, M. Q.; Haussler, L.; Thranert, S.; Hassan, E. M.; Krause-Rehberg, R. *e-Polym.* **2007**, *108*, 1–20.
(37) Nagel, C.; Schmidtke, E.; Gunther-Schade, K.; Hofmann, D.; Fritsch, D.; Strunskus, T.; Faupel, F. *Macromolecules* **2000**, *33*, 2242–2248.
(38) Jameson, C. J.; Lim, H. M.; Jameson, A. K. *Solid State Nucl. Magn. Reson.* **1997**, *9*, 277–301.
(39) Bifone, A.; Pietrass, T.; Kritzenberger, J.; Pines, A.; Chmelka, B. F. *Phys. Rev. Lett.* **1995**, *74*, 3277–3280.
(40) Demarquay, J.; Fraissard, J. *Chem. Phys. Lett.* **1987**, *136* (3−4), 314–318.
(41) Koskela, T.; Jokisaari, J.; Satyanarayana, C. *Microporous Mesoporous Mater.* **2004**, *67* (2−3), 113–122.
(42) Golemme, G.; Nagy, J. B.; Fonseca, A.; Algieri, C.; Yampolskii, Y. *Polymer* **2003**, *44*, 5039–5045.
(43) Menge, H.; Kühn, H.; Blümich, B.; Blümler, P.; Schneider, H. *Macromol. Mater. Eng.* **2000**, *282* (1), 1–4.
(44) Yampolskii, Y. P. *Russ. Chem. Rev.* **2007**, *76* (1), 59–78.
(45) Budd, P. M.; McKeown, N. B.; Ghanem, B. S.; Msayib, K. J.; Fritsch, D.; Starannikova, L.; Belov, N.; Sanfirova, O.; Yampolskii, Y.; Shantarovich, V. *J. Membr. Sci.* **2008**, *325*, 851–860.
(46) Niederl, J. B.; Nagel, R. H. *J. Am. Chem. Soc.* **1940**, *62*, 3070–3072.
(47) Horvath, G.; Kawazoe, K. *J. Chem. Eng. Jpn.* **1983**, *16*, 470–475.
(48) Kruse, J.; Kanzow, J.; Ratzke, K.; Faupel, F.; Heuchel, M.; Frahn, J.; Hofmann, D. *Macromolecules* **2005**, *38*, 9638–9643.
(49) Kansy, J. *Nucl. Instrum. Methods Phys. Res., Sect. A* **1996**, *374*, 235–244.
(50) Tao, J. C.; Sandler, S. I.; Ganzi, G. C. *J. Chem. Phys.* **1972**, *56*, 3789.
(51) Eldrup, M.; Lightbody, D.; Sherwood, J. N. *Chem. Phys.* **1981**, *63* (1−2), 51–58.
(52) Jean, Y. C. *Microchem. J.* **1990**, *42* (1), 72–102.
(53) Rudel, M.; Kruse, J.; Rätzke, K.; Faupel, F.; Yampolskii, Y. P.; Shantarovich, V. P.; Dlubek, G. *Macromolecules* **2008**, *41*, 788–795.
(54) Dlubek, G.; Pionteck, J.; Rätzke, K.; Kruse, J.; Faupel, F. *Macromolecules* **2008**, *41*, 6125–6133.
(55) Dlubek, G.; Pionteck, J.; Yu, Y.; Thranert, S.; Elsayed, M.; Badawi, E.; Krause-Rehberg, R. *Macromol. Chem. Phys.* **2008**, *209*, 1920–1930.
(56) Tokarev, A. V.; Bondarenko, G. N.; Yampolskii, Y. P. *J. Polym. Sci., Ser. A: Polym. Phys.* **2007**, *49*, 909–920.
(57) Feng, H. D. *Polymer* **2007**, *48*, 2988–3002.
(58) Platé, N. A.; Bokarev, A. K.; Kaliuzhnyi, N. E.; Litvinova, E. G.; Khotimskii, V. S.; Volkov, V. V.; Yampolskii, Y. P. *J. Membr. Sci.* **1991**, *60* (1), 13–24.
(59) Volkov, V. V. *Polym. J.* **1991**, *23*, 457–466.
(60) Merkel, T. C.; Toy, L. G.; Andrady, A. L.; Gracz, H.; Stejskal, E. O. *Macromolecules* **2003**, *36*, 353–358.
(61) Bansal, N.; Foley, H. C.; Lafyatis, D. S.; Dybowski, C. *Catal. Today* **1992**, *14*, 305–316.
(62) Sams, J. R.; Constabaris, G.; Halsey, G. D. *J. Phys. Chem.* **1960**, *64*, 1689–1696.
(63) Hobson, J. P. *J. Phys. Chem.* **1969**, *73*, 2720–2727.
(64) Patterson, H. S.; Cripps, R. S.; Whytlaw-Gray, R. *Proc. R. Soc. London, Ser. A* **1912**, *86* (591), 579–590.
(65) Suzuki, T.; Miyauchi, M.; Yoshimizu, H.; Tsujita, Y. *Polym. J.* **2001**, *33*, 934–938.
(66) Paterson, R.; Yampolskii, Y.; Fogg, P. G. T.; Bokarev, A.; Bondar, V.; Ilinich, O.; Shishatskii, S. *J. Phys. Chem. Ref. Data* **1999**, *28*, 1255–1450.
(67) Fraissard, J.; Ito, T. *Zeolites* **1988**, *8*, 350–361.
(68) Miller, J. B.; Walton, J. H.; Roland, C. M. *Macromolecules* **1993**, *26*, 5602–5610.
(69) Wang, Y.; Inglefield, P. T.; Jones, A. A. *Polymer* **2002**, *43*, 1867–1872.
(70) Simpson, J. H.; Wen, W. Y.; Jones, A. A.; Inglefield, P. T.; Bendler, J. T. *Macromolecules* **1996**, *29*, 2138–2142.
(71) Nagasaka, B.; Eguchi, T.; Nakayama, H.; Nakamura, N.; Ito, Y. *Radiat. Phys. Chem.* **2000**, *58*, 581–585.
(72) Suzuki, T.; Yoshimizu, H.; Tsujita, Y. *Desalination* **2002**, *148* (1−3), 359–361.
(73) Suzuki, T.; Yoshimizu, H.; Tsujita, Y. *Polymer* **2003**, *44*, 2975–2982.
(74) Ripmeester, J. A.; Ratcliffe, C. I.; Tse, J. S. *J. Chem. Soc., Faraday Trans. 1* **1988**, *84*, 3731–3745.
(75) Ito, T.; Springuelhuet, M. A.; Fraissard, J. *Zeolites* **1989**, *9* (1), 68–73.
(76) Ripmeester, J. A.; Ratcliffe, C. I. *J. Phys. Chem.* **1990**, *94*, 7652–7656.
(77) Breck, D. W., *Zeolite molecular sieves: structure, chemistry, and use*; Wiley: New York, 1973.